HHS Public Access

Author manuscript

Mol Cancer Res. Author manuscript; available in PMC 2020 December 01.

Published in final edited form as:

Mol Cancer Res. 2020 June ; 18(6): 913–925. doi:10.1158/1541-7786.MCR-19-0726.

Cdc42 mediates cancer cell chemotaxis in perineural invasion

Natalya Chernichenko[1], **Tatiana Omelchenko**[2], **Sylvie Deborde**[1], **Richard Bakst**[3], **Shizhi He**[1], **Chun-Hao Chen**[1], **Laxmi Gusain**[1], **Efsevia Vakiani**[4], **Nora Katabi**[4], **Alan Hall**[2,*], **Richard J Wong**[1]

[1]Department of Surgery, Memorial Sloan-Kettering Cancer Center, New York, NY, 10021

[2]Cell Biology Program, Memorial Sloan-Kettering Cancer Center, New York, NY, 10021

[3]Department of Radiation Oncology, Mount Sinai Hospital, New York, NY, 10029

[4]Department of Pathology, Memorial Sloan-Kettering Cancer Center, New York, NY, 10021

Abstract

Perineural invasion (PNI) is an ominous form of cancer progression along nerves associated with poor clinical outcome. Glial derived neurotrophic factor (GDNF) interacts with cancer cell RET receptors to enable PNI, but downstream events remain undefined. We demonstrate that GDNF leads to early activation of the GTPase Cdc42 in pancreatic cancer cells, but only delayed activation of RhoA and does not affect Rac1. Depletion of Cdc42 impairs pancreatic cancer cell chemotaxis towards GDNF and nerves. An siRNA library of guanine nucleotide exchange factors was screened to identify activators of Cdc42. ARHGEF7 (β-Pix) was required for Cdc42 activation and chemotaxis towards nerves, and also co-localizes with RET under GDNF stimulation. Cdc42 enables PNI in an *in vitro* dorsal root ganglia (DRG) co-culture model, and controls the directionality of migration but does not affect cell speed or cell viability. In contrast, Rac1 was necessary for cell speed but not directionality, while the RhoA was not necessary for either cell speed or directionality. Cdc42 was required for PNI in an *in vivo* murine sciatic nerve model. Depletion of Cdc42 significantly diminished the length of PNI, volume of PNI, and motor nerve paralysis resulting from PNI. Activated Cdc42 is expressed in human salivary ductal cancer cells invading nerves. These findings establish the GDNF-RET-β-Pix-Cdc42 pathway as a directional regulator of pancreatic cancer cell migration towards nerves, highlight the importance of directional migration in PNI, and offer novel targets for therapy.

Introduction

Perineural invasion (PNI) is defined as tumor cell invasion in, around and through nerves (1). The extension of cancer cells along nerves is an adverse clinical, radiographic, and pathologic finding for a variety of cancer types, including pancreatic, head and neck,

Correspondence: Richard J. Wong, MD, Memorial Sloan-Kettering Cancer Center, 1275 York Avenue, C-1069, New York, NY 10021, Office: (212) 639-7638, FAX: (212) 717-3302, wongr@mskcc.org.

*Deceased

The authors declare that they each do not have any conflict of interest with the material in this manuscript.

Conflict of Interest

The authors all declare no conflict of interest with the content of this manuscript.

cervical, prostate, colorectal, stomach, and others (2–10). PNI is a marker of poor clinical outcome, and is associated with an increased risk of cancer recurrence, a shorter time to recurrence, and diminished patient survival (2–10). PNI may induce patient morbidity resulting from nerve dysfunction, leading to pain, paralysis, weakness, and numbness. The specific molecular mechanisms of PNI remain poorly understood. Developing a mechanistic understanding of PNI may facilitate the identification of novel targets and therapeutic approaches.

Recent studies suggest that PNI is a complex event resulting from reciprocal signaling and interactions between cancer cells, nerves, and stromal cells (2–3). Nerves and their supporting cells secrete chemokines and growth factors that play important roles in neural development, proliferation, and repair. One such factor is glial cell line derived neurotrophic factor (GDNF) which signals through the RET tyrosine kinase receptor and its glycosyl-phosphatidylinositol-anchored co-receptor, GFRα1 (11). GDNF plays an essential role in the development, function and regeneration of the nervous system. GDNF and GFRα1 released by nerves activate the RET receptor expressed by cancer cells, inducing migration towards nerves and supporting PNI (12–14).

However, the downstream molecular mechanisms through which GDNF induces migration of cancer cells remain unclear. Activation of the MAPK and PI3K pathways have in pancreatic cancer cell lines has been implicated in this process (12, 14). Rho GTPases are regulators of actin polymerization, cell polarity, and directional migration (15–16). During chemotaxis, the activity of three Rho GTPases (Cdc42, Rac1 and RhoA) is temporally and spatially controlled. Cdc42 at the leading edge of a migrating cell links extracellular cues to directional sensing, and activates pathways that localize Rac1 to the leading edge of the cell. The accumulation of Rac1 and Cdc42 at the leading edge of the migrating cell of facilitates the protrusion of lamellipodia and filopodia, respectively, promoting forward cell migration. RhoA acts at the rear of the cell to generate contractile forces through ROCK, which facilitate retraction of the rear of the cell (15–16). Rac1 and RhoA may be dysregulated in highly motile cancer cells, although mutations in these genes are rarely found (17–19). Rho GTPase activity has been linked to malignant transformation and the induction of invasive and metastatic programs (20–22).

We sought to examine the role of Rho GTPase activity in PNI. We demonstrate here that GDNF-mediated activation of RET leads to activation of the Rho GTPase Cdc42 as a mediator of directional migration that is required for cancer cell chemotaxis and perineural invasion. Furthermore, we identify and validate β-Pix as a regulator of Cdc42 activation in this system. These results establish that the GDNF-RET-β-Pix-Cdc42 signaling pathway drives PNI, highlight the mechanistic importance of directional migration in this form of cancer progression, and offer novel therapeutic targets to potentially interrupt this process.

Materials and Methods

Cell lines, reagents and transfections

The human pancreatic carcinoma cell line (MiaPaCa2) and human colonic epithelial cell line (Caco2) were purchased from ATCC. The cell lines used were passaged no more than 20

times and underwent mycoplasma testing every 3 months by Hoechst staining. GDNF was obtained from EMD Chemicals (Rockland, MA). MiaPaCa2 cells were transfected with (1) siGENOME SMARTpool siRNA (Dharmacon/Thermo Scientific) targeting human Cdc42 (M-005057-01), (2) siGENOME SMARTpool targeting human RhoA (M-003860-03), (3) ARHGEF7 siGENOME individual duplexes (D-009616-01, D-009616-02, D-009616-03, D-009616-04), and (3) siRNA targeting Rac1 (NM 018890, human), to the sequence: GAA GAU UAU GAC AGA UUA CTT (MWG Biotech/Operon) using Oligofectamine Transfection Reagent (Invitrogen). siLaminA/C (Dharmacon/Thermo Scientific) was used as a control. Cell morphology was assessed seventy-two hours post-transfection. Plasmids encoding shRNA targeting the sequence CCTGATATCCTACACAACAAA (TRCN0000047630) and the sequence CGGAATATGTACCGACTGTTT (TRCN0000047629) to silence Cdc42 were purchased from Sigma-Aldrich. The pLKO.1 empty vector was used as a negative control.

Antibodies, western blots, immunofluorescence microscopy

Primary antibodies were obtained targeting: Cdc42 (rabbit polyclonal, Cell Signaling), Rac1 (mouse monoclonal, Cytoskeleton), RhoA (mouse monoclonal, Santa Cruz), β-Pix (rabbit polyclonal, Millipore), Tuj1 (mouse monoclonal, Millipore), active Cdc42 (mouse monoclonal, New East Biosciences), Ret (pig anti-human, Abgent). The secondary antibodies used included: goat anti-mouse (Santa Cruz) and goat anti-rabbit (Santa Cruz). For western blots, cells were lysed with RIPA buffer (SantaCruz), boiled and separated by 3-8% Tris-Acetate SDS-PAGE.

For immunofluorescence microscopy, antibodies used included RET (rabbit monoclonal, Cell Signaling), p-Ret (phospho-Y1062, rabbit polyclonal, Abcam), β-pix (SH3 domain, rabbit polyclonal, Millipore Sigma), and Cdc42 (rabbit polyclonal, Cell Signaling). Cells were fixed in 4% formaldehyde and permeabilized in 0.5% Triton X-100 (vol/vol), or fixed in 3.7% paraformaldehyde and blocked with 3% horse serum in 0.1% Triton in PBS for 60 minutes. The secondary antibody was Alexa Fluor 488 (goat anti-rabbit, Thermo Fisher Scientific). Slides were mounted with ProLong Diamond Antifade Mountant (Invitrogen, Thermo Fisher Scientific) and were scanned with a Flash Scanner (Perkin Elmer) and a Panoramic Viewer (3DHistech, Thermo Fisher Scientific) was used to capture images.

Dorsal root ganglia (DRG) preparation

Mice were maintained according to NIH animal care guidelines under a protocol approved by the MSKCC Institutional Animal Care and Use Committee. Mice (Balb/c, 2-4 weeks old) were euthanized by CO2 inhalation. DRG were isolated as previously described (12–13, 23, 25) and washed in phosphate buffered saline (PBS) prior to implantation into growth factor-depleted Matrigel matrix (BD Biosciences, Bedford, MA) for Boyden chamber or DRG co-culture assays.

Activity of monomeric GTPases

Serum starved cells were exposed to 100 ng/ml of GDNF for varying time periods. The GTP-bound forms of Cdc42, Rac1 and RhoA were recovered from cell lysates by affinity precipitation using glutathione S-transferase (GST)-fusion proteins carrying the GTP-

binding domains of GTPase-specific effector proteins (ThermoScientific, Pierce). GST-PBD (p21-binding domain of Pak1) was used to recover Cdc42 and Rac1, and GST-RBD (Rho-binding domain of rhotekin) was used to recover Rho. Proteins were detected by SDS-PAGE and immunoblot. Western blot results were quantified based on intensity by MetaMorph software.

Boyden chamber migration assay

Polyethylene terephthalate 8.0 μm pore inserts (BD Biosciences, Bedford, MA) were used in 24-well plates. Cancer cells were incubated in 0.1% FCS media overnight, and $2x10^5$ cells were added to each of the inserts. The attractants used included: (1) 0.7 ml of 100 ng/mL GDNF in 0.1% FCS media, (2) DRG in 0.1% FCS media, or (3) 0.1% FCS media as control. Inserts were removed after 24 hours, and non-migrating cells wiped off the superior aspect of the membrane. Migrating cells on the undersurface of the membrane were fixed in 100% alcohol and stained with 1% methylene blue in 1% borax. Membranes were excised and mounted on a glass slides. Cells were quantified by counting stained cells in five high-power fields at predetermined areas.

Dorsal root ganglion (DRG) co-culture model to assess nerve cancer cell interactions

DRG in Matrigel drops were incubated in DMEM containing 10% FCS. After 7 days, cancer cells were added in 0.1% FCS DMEM (Figure 3A). Dynamic interactions between cancer cells and neurites were studied by time-lapse microscopy. Digitalized images were recorded every 5 min for up to 24 hours to follow cell locomotion. Image analysis was performed using MetaMorph software. X-Y coordinates were determined of individual cells at each time point, allowing for calculations of distance travelled, average speed, and trajectory plotting of each cell. The area of cancer invasion in the DRG was quantified at 48 hours as a late measure of perineural invasion. A GFP expressing MiaPaCa2 cell line, generated by pQXIP GFP infection, was transfected with siRNA targeting Cdc42 or Rac1 and co-cultured with DRG. Confocal microscopy images were acquired with LSM5 Live Duoscan (Carl Zeiss Microimaging) equipped with 10x 0.45 NA Carl Zeiss objective lens. Areas of DRG invasion by GFP positive cells were measured with Metamorph software.

siRNA screen of guanine exchance factors necessary for cell migration and Cdc42 activation

MiaPaCa2 cells were transfected with individual SMART-pool siRNAs (Dharmacon / Thermo Scientific) targeting 79 different guanine exchange factors (GEFs) using oligofectamine. Boyden chamber migration assays using DRG as an attractant were performed to identify GEFs required for migration. Cell viability assays were performed with trypan blue staining and a Z1 Coulter Particle Counter (Beckman Coulter). GEFs required for cell viability or proliferation were excluded.

A Cdc42 activity assay following GDNF exposure was also used to screen GEF candidates. MiaPaCa2 cells transfected with siRNA were starved and were stimulated with 100 ng/ml GDNF for 5 minutes. Lysates were assessed using the G-linked immunosorbent assay (G-LISA) kit for Cdc42-GTP (Cytoskeleton). The ratio of Cdc42-GTP with and without GDNF stimulation was calculated for each GEF silenced.

Co-localization of β-Pix and RET by immunofluorescence microscopy

β-Pix and RET localization was assessed by immunofluorescence microscopy in Caco2 cells. β-Pix and RET are difficult to localize by IF in MiaPaCa2 cells, and overexpression of these proteins in MiaPaCa2 leads to cell death (data not shown). In contrast, human colon cancer Caco2 cells were receptive to nucleofection with HA tagged β-Pix, and GFP tagged RET. Cells were starved in serum free DMEM overnight, exposed to GDNF for 15 min, and fixed in formaldehyde. β-Pix was detected using an anti-HA mouse primary antibody (Covance) and a secondary donkey anti-mouse Cy3 antibody (Jackson Immunoresearch). RET was detected by imaging GFP signal. Images were obtained with epifluorescent microscopy. Co-localization of GFP-RET and HA-β-Pix signals was analyzed by utilizing Metamorph.

β-Pix and RET proximity ligation assay

Caco-2 cells expressing HA-β-Pix and GFP-RET were grown on glass coverslips, starved in serum free medium for 24h, fixed with 3.7% formaldehyde, permeabilized in 0.5% Triton X-100 and blocked with 10% fetal bovine serum in PBS. Proximity ligation *in situ* assays were performed using the Duolink II kit (Olink Bioscience, Uppsala, Sweden). Cells were incubated with anti-HA Mouse antibody (MMS-101R, clone 16B12, Covance) or anti-GFP rabbit antibody (A11122, Molecular Probes), followed by incubation with secondary antibodies conjugated with PLA probes (anti-Goat MINUS or anti-Rabbit PLUS). Ligation and amplification were performed, and images obtained with epifluorescent microscopy. Puncta were counted using MetaMorph software, with thresholded signal sizes ranging from 0.5-2.5 μm.

In vivo murine model of sciatic nerve function

Nude athymic mice (n=5 per group) were anesthetized with isoflurane and their sciatic nerves surgically exposed. Control transfected (pLKO.1 empty vector) and shCdc42 MiaPaCa2 cell lines (3 μL, $1x10^5$ cell/μL) were injected into the sciatic nerves under magnification using a 10 μL Hamilton syringe. Nerve function was measured immediately after the injection and weekly thereafter (30). Using the *sciatic neurologic score*, nerve function is graded according to hind limb paw response to manual extension of the body, from 5 (normal) to 1 (total paralysis). Using the *sciatic nerve function index*, the spread width between the first and fifth toes of the mouse hind limb is measured. Sciatic nerve tumors generated from control and shCdc42 MiaPaCa2 cell lines were excised, frozen in Tissue Tek OCT (Sakura FInetek USA), and sectioned at 8 μm thickness for immunofluorescence microscopy as described above.

MRI imaging of perineural invasion in vivo

Anesthetized mice underwent magnetic resonance imaging (MRI) on a Bruker USR 4.7T 40-cm bore scanner (Bruker Biospin MRI, Ettingen, Germany) equipped with 400 mT/m 12-cm bore gradient using a custom active decoupled radiofrequency surface coil (Stark MRI Contrast Research, Erlangen, Germany). A scout fast spin echo scan in three orientations was acquired to localize the sciatic nerve, followed by an oblique-coronal T2-weighted fast spin-echo image. Contrast was injected via mouse-tail vein 0.1 mmol/kg Gd-DTPA

(gadolinium diethylenetriamine penta-acetic acid). Oblique-coronal T1-weighted gradient-echo images were acquired continuously pre- and post-injection. Tumor volume at the injection site, volume and length of PNI were quantified with Paravision software.

Immunohistochemistry of human neuroinvasive cancer

Studies on human tissue samples were under a protocol approved by the MSKCC Institutional Review Board. Patients underwent surgical specimen collection after planned surgical resection of salivary ductal carcinoma. Specimens were embedded in Optimum Cutting Temperature compound (Miles Inc.) rapidly frozen in liquid nitrogen. Sections were stained with hematoxylin and eosin and assessed for the presence of nerve cancer infiltration. Immunostaining with anti-GTP-Cdc42 was performed with a Ventana automated staging system (Ventana Medical Systems, Tucson, AZ).

Statistical analysis

Two tailed paired t-tests were performed to test for statistical significance, using 95% confidence intervals.

Results

Activation of Rho GTPases by glial cell line derived neurotrophic factor (GDNF)

The MiaPaCa2 pancreatic cancer cell line invades nerves in co-culture *in vitro* assays with dorsal root ganglia (DRG), and following *in vivo* injection into murine sciatic nerves (12–13). We assessed if GDNF exposure affects the activity of Rho GTPases in MiaPaCa2 cells. GDNF stimulation at 5 minutes resulted in phenotypic changes observed using a rhodamine-phalloidin stain (Figure 1A), showing the formation of microspikes, filopodia, and prominent stress fibers. The levels of the activated (GTP-bound) Rho GTPases (Cdc42, Rac1, RhoA) were measured by affinity precipitation using GST-fusion proteins carrying the GTP-binding domains of GTPase-specific effector proteins. The addition of GDNF (100ng/ml) to serum-starved MiaPaCa2 cells induced a rapid and transient activation of Cdc42 beginning at 1 minute (Figure 1B). Rac1 appeared activated already at baseline for MiaPaCa2 cells, and there was a slight reduction in the activation level of Rac1 with GDNF exposure (Figure 1C). RhoA activation was activated by GDNF but in delayed manner fashion with maximal stimulation at 30 minutes (Figure 1D).

Cdc42 and Rac1 silencing impairs GDNF dependent chemotaxis

To investigate the effects of Rho GTPase depletion on cancel cell phenotype, we performed transient siRNA knockdown of Cdc42, Rac1 and RhoA (Figure 2C). Depletion of these Rho GTPases in MiaPaCa2 cells results in a change in cell morphology. Cdc42 silencing results in the development of lamellipodial protrusions in all directions around the cell periphery, without any directional preference. In contrast, Rac1 silencing blocks the formation of all lamellipodial protrusions. RhoA silencing results in tail formation, likely from an inability of the cell to retract its trailing rear (Figure 2A).

We assessed how Rho GTPase silencing affects GDNF dependent chemotaxis in Boyden chamber migration assays. GDNF induces MiaPaCa2 cell migration in a dose-dependent

fashion through RET receptor signaling (12–14). More robust migration is seen when live explants of murine dorsal root ganglia (DRG) are used as the chemoattractant. DRG actively produce GDNF, along with other potential neurotrophic factors including CCL2 (23). Cdc42 or Rac1 silencing impairs chemotaxis towards DRG as compared with either MiaPaCa2 or siLamin A/C as control ($p<0.05$ for all comparisons, t-test), while RhoA depletion has no effect (p=NS) without impairing cell proliferation (Figure 2B). In contrast, RhoA silencing demonstrates no effect on chemotaxis towards either GDNF or DRG (Figure 2B).

siRNA screen of GEFs mediating cancer chemotaxis towards DRG

Guanine exchange factors (GEFs) activate Rho GTPases in response to diverse extracellular stimuli (15–17). A comprehensive siRNA screen of 79 different guanine nucleotide exchange factors (GEFs) was performed to identify factors necessary for Cdc42-mediated MiaPaCa2 chemotaxis to DRG in a Boyden chamber assay. The silencing of 23 individual GEFs was found to impair cancer chemotaxis (Fig. 3A). Ten of these GEFs were essential for cell proliferation (Fig. 3B), and were excluded. Silencing of ECT2 resulted in a multinucleated cell phenotype and was also excluded.

We next assessed how silencing the remaining 12 GEFs would affect the ability of GDNF to activate Cdc42. Using a G-linked immunosorbent assay (G-LISA) to assess Cdc42 activity, we identified 6 GEFs as candidate activators of Cdc42 in response to GDNF (Fig. 3C). Each of these GEFs supports MiaPaCa2 chemotaxis towards DRG and GDNF-mediated Cdc42 activation, but is not required for cell proliferation.

ARHGEF7 (β-Pix) co-localizes with RET under GDNF stimulation

From these candidates, ARHGEF7 (β-Pix), an activator of Cdc42, was selected for further evaluation. G-LISA demonstrated that the amount of activated Cdc42 was diminished in GDNF-stimulated MiaPaCa2 with treatment by siRNA targeting β-Pix or Cdc42 (Figure 4A). Significant differences in active GTP-Cdc42 between siLamin A/C and siCdc42 ($p<0.05$, t-test), and between siLamin A/C and si-β-pix ($p<0.05$, t-test) were identified. Four different siRNA duplexes were used to validate that the silencing of β-Pix consistently leads to an inhibition of MiaPaCa2 cell migration towards DRG in Boyden chamber assays as compared with siLamin A/C ($p<0.05$, all comparisons, t-test, Figure 4B). Western blot confirmed depletion of β-Pix by each of these four siRNA duplexes (Figure 4C).

GDNF acts through stimulation of the RET receptor (12,14). To assess for a direct interaction between GDNF-RET binding and β-Pix, we next directly assessed β-Pix and RET co-localization following GDNF stimulation by immunofluorescence microscopy in Caco2 cells transfected with both proteins. The transfection of β-Pix and RET into MiaPaCa2 led to cell death, but the human colonic epithelial Caco2 cell line was receptive to transfection of these two proteins. At baseline, β-Pix and RET do not associate with one another. However, under GDNF stimulation, β-Pix and RET co-localize together, suggesting functional interactions between the two proteins when RET is activated (Figure 4D). Next, Duolink proximity ligation experiments were performed to corroborate direct interactions between β-Pix and RET. Under GDNF stimulation, β-Pix and RET again associated together in close proximity, as demonstrated by PLA probe fluorescence ($p<0.05$, t-test, Figure E-F).

These results suggest that RET and β-Pix interact together to mediate Cdc42 activation after GDNF stimulates the RET receptor.

Cdc42 regulates cancer migration directionality and Rac1 cancer migration speed along nerves in vitro

We investigated the effects of Cdc42 and Rac1 depletion on cancer cell migration using an *in vitro* model of PNI. In this model, explants of murine DRG grown in Matrigel are co-cultured together with cancer cells (Figure 5A). Neurites are axonal projections analogous to small nerves that sprout from the DRG explants. Cancer cells exhibiting perineural invasive behavior associate with neurites and migrate along them towards the ganglion (12–13, 23–25). The process through which cancer cells invade DRG was captured by time-lapse microscopy (Figure 5B). Each individual cell's migratory path was tracked and its velocity calculated.

The control (siLaminA/C) MiaPaCa2 cells consistently associate with the DRG neurites and migrate in a linear, unidirectional fashion along the neurites towards the center of the ganglion, leading to invasion of the DRG (Figure 5C). In contrast, siCdc42 MiaPaCa2 cells continue to migrate, but have lost directionality in their migration pattern and move in random patterns and directions (Figure 5D). These cells fail to consistently associate with or migrate along the DRG neurites. They maintain an intact speed of migration (Figure 5F), although this migration is without a consistent direction. In contrast, the siRac1 MiaPaCa2 cells exhibited significantly reduced overall cell motility and a diminished speed of migration (Figure 5F). These cells were unable to either associate with or migrate along the DRG neurites (Figure 5E).

The degree of perineural invasion was quantified by measuring the area of PNI, defined as areas where the cancer cells are in direct contact with DRG neurites, using Metamorph software (13, 23, 25). Both siCdc42 ($p=0.08$) and siRac1 MiaPaCa2 cells ($p=0.07$) demonstrated a trend towards a reduction in the area of PNI as compared with control siLaminA/C MiaPaCa2 cells (Figure 5G). These findings demonstrate that the loss of migratory ability, either through impaired directionality (siCdc42) or through impaired velocity (siRac1), correlates with a diminished PNI phenotype in this model.

Cdc42 regulates perineural invasion of cancer cells in vivo

We optimized an orthotopic murine sciatic nerve model that allows for the radiographic, pathologic, and functional assessment of PNI *in vivo* (12–13, 23, 25). We generated MiaPaCa2 cell lines stably expressing two different shRNA targeting Cdc42 (Figure 6F), or empty vector transfected control. Cancer cells were injected into the distal sciatic nerve (Figure 6A), and sciatic nerve function was assessed over time by two methods: (*i*) the hind limb motor response to manual extension (sciatic nerve function score) and (*ii*) the spread width between the digits of the hind paw (sciatic nerve index).

In the control group, mice began to develop left hind limb weakness 4 weeks after tumor implantation (Figure 6B). Mean scores for sciatic nerve function score show a significant decline over 6 weeks for the control group ($p<0.05$, t-test), but not for the shCdc42 groups (p=NS). Similarly, the control group showed a significant decline in sciatic nerve index

(p<0.05, t-test), but not for the chCdc42 groups (p=NS). To account for differential growth rates, comparisons were made between equivalent tumor volumes between week 6 data for the control group, and week 7 in the shCdc42 groups.

Magnetic resonance imaging (MRI) was used to non-invasively measure the tumor volume and the length of PNI in live mice. Cdc42 silencing results in slightly slower tumor growth than control. To account for this potential confounder, MRI imaging was compared at different time points when the mean primary tumor volume was equivalent for each of the experimental groups: week 6 data for the control group and week 7 for both of the experimental groups (Figure 6D, left panel). MRI revealed control tumors extending longitudinally along the course of a thickened sciatic nerve, while in contrast the shCdc42 tumors grew in a spherical shape at the site of injection without evidence of PNI (Figure 6C). Image assessment of the length and volume of tumor invading the sciatic nerve revealed a significant decreases in both of these measures of PNI for both shCdc42 groups as compared to control (p<0.05 for both comparisons, t-test, Figure 6D, middle and right panels).

Animals were sacrificed after week 7 for examination of the sciatic nerves. Control tumor mice demonstrated gross nerve thickening and infiltration by tumor, with extension of tumor proximally towards the spinal cord. In contrast, shCdc42 tumors remained localized to the implantation site, expanding spherically as primary tumors but failing to invade along the sciatic nerves, which remained intact as thin, white structures (Figure 6E). Immunofluorescence microscopy demonstrates increased Cdc42, β-Pix, and p-RET expression for control tumors as compared with shCdc42 tumors, while total RET expression remained unchanged (Supplementary Figure). Immunohistochemistry demonstrates robust GTP-Cdc42 expression in control tumors (Supplementary Figure).

GTP-Cdc42 is expressed in human carcinomas with perineural invasion

Immunohistochemistry was performed on fresh frozen human surgical specimens of two human carcinomas to assess for GTP-Cdc42 expression. One salivary ductal carcinoma of the parotid gland exhibited PNI of the facial nerve, causing a preoperative facial nerve paralysis. A second salivary ductal carcinoma lacking PNI was assessed in comparison. Nerve infiltration by cancer cells was confirmed with hematoxylin and eosin (H&E) staining. Immunohistochemical staining revealed robust expression of activated GTP-Cdc42 by human salivary ductal cancer cells that are invading nerves, but a lack of expression of GTP-Cdc42 in human salivary ductal cancer cells lacking any association with nerves (Figure 7).

Discussion

The identification of a cancer invading and tracking along nerves is an ominous finding that heralds poor clinical outcomes (1–10). PNI allows cancers to extend insidiously and unpredictably along both sensory and motor nerves, tracking away from the primary tumor, often in a proximal direction towards the central nervous system. PNI represents a unique type of cancer behavior that is poorly understood, distinct from commonly recognized modes of cancer progression such as lymphatic and hematogenous metastases. PNI causes

morbidity from pain and paralysis, and is a pathologic feature that is associated with a higher disease recurrence risk and a worse survival rate (2–10). Despite widespread recognition of the significance of this process, the mechanisms underlying PNI remain poorly defined.

Recent studies point to the active role that the tumor microenvironment plays in PNI, and demonstrate that PNI results from reciprocal signaling interactions between cancer cells, stromal cells and nerve cells (2–3). Both Schwann cells and monocytes have been shown to play an important role in enabling PNI (26–27). Importantly, PNI is facilitated by neural release of GDNF, which activates the RET tyrosine kinase receptor and induces cancer cell migration towards nerves and PNI (12, 14). Either neutralizing antibodies against GDNF or RET inhibitors are able to inhibit MiaPaCa2 cell recruitment by murine dorsal root ganglia (12). In addition, GFRα is released in a soluble form by nerves to further support GDNF-RET signaling and PNI (13). However, the specific downstream signaling events within the cancer cell following RET phosphorylation that then drive directional migration towards GDNF were unclear.

Cell migration is a fundamental process that is important for embryogenesis, immune surveillance, and wound healing. Chemotaxis occurs when an external soluble factor asymmetrically dictates the direction of cell migration. Studies of chemotaxis have using *Dictostelium discoideum* and have demonstrated that the temporal regulation of PI3K at the leading edge of cells plays an important role in mediating chemotaxis (28). Rho GTPases have been shown to play key roles in cell migration (19). Rac, acting through WAVE and Arp2/3, promotes actin polymerization at the leading edge of migrating cells (16). RhoA acts at the rear of the cell to generate contractile forces that retract the tail of the cell (29). Cdc42 is a regulator of cell polarity (30) that influences directional migration, linking external cues to activation of Rac1 and Arp2/3 (16). Cdc42 activates atypical protein kinase C, PAR3 and PAR6 at the leading edge of the cell to stabilize microtubules and promote directional migration (31). Cdc42 is involved in regulating mesenchymal and ameboid types of movement, and may be overexpressed by some cancer cells (32). Although Cdc42 plays a role in macrophage chemotaxis (33), its role in cancer cell directional migration is less well established (34). Cdc42 plays a role in enabling cancer cells to follow leading invading fibroblasts (35), and in transendothelial cancer cell migration (22).

We investigated the role of Rho GTPases in PNI using a Boyden chamber assay, a dorsal root ganglia (DRG) co-culture model and an *in vivo* murine sciatic nerve model. These models have previously been shown to depend upon GDNF-RET mediated signaling (12–13). We found that both RhoA and Cdc42 were activated in MiaPaCa2 cells by GDNF stimulation, while Rac1 was already active prior to GDNF exposure. The depletion of Cdc42 or Rac1, but not RhoA, led to an inhibition of chemotaxis in Boyden chamber assays. We sought to identify the activators of Cdc42. Receptor TKs initiate intracellular signaling to Rho proteins through GEFs, although one that couples RET-Cdc42 signaling had not been previously reported. We identified and validated ARHGEF7 (β-Pix) (36–37) as a GEF that is required for cancer cell migration towards DRG, activates Cdc42 in response to GDNF, but is non-essential to proliferation. In addition, we demonstrate that β-Pix co-localizes with RET under GDNF stimulation.

In DRG co-culture assays, the depletion of Rac1 diminished cell speed and migration. In contrast, the depletion of Cdc42 led to a loss of directional migration, but these cells maintained intact speed and a random pattern of migration. To assess the effects of Cdc42 on PNI in an animal model, we used a stably repressed Cdc42 cell line to generate tumors within murine sciatic nerves. This model allows for the study of PNI in large caliber nerves, and also accounts for the contributions of supporting glial cells, vessels, immune cells, and other factors in the nerve microenvironment. The depletion of Cdc42 significantly diminished PNI as measured by nerve function, MRI imaging, and histology. These findings establish Cdc42 as a regulator cancer cell directional migration that is required for perineural invasion.

These results suggest that GDNF activates cancer cell RET, which interacts with β-Pix to activate Cdc42 as a regulator of cell migration directionality and support PNI in these pancreatic cancer models. These results highlight the importance of directional cell migration as a key process that is fundamental to perineural invasion. We found that that Cdc42 is central for cancer cell chemotaxis in enabling cancer cells to directionally migrate towards neural sources of GDNF, such as Schwann cells. The Neural Wiskott-Aldrich syndrome protein (N-WASP) transmits signals from Cdc42 to actin filaments through the ARP2/3 complex, supporting actin polymerization and formation of cell protrusions (38). Interestingly, increased expression of N-WASP by immunohistochemistry has been associated with PNI in human pancreatic cancer tissue specimens (39), further supporting this model.

These findings provide novel insights into the molecular mechanisms underlying PNI. The nerve microenvironment emits a molecular signal to attract Cdc42-dependent directional cancer cell migration to the nerve. This interplay between cancer cell migration and the nerve microenvironment involves the GDNF-RET-β-Pix-Cdc42 signaling pathway, and may be potentially interrupted with pharmacologic agents targeting its components. Novel therapeutic approaches to targeting PNI may potentially impede a highly aggressive form of cancer progression and improve clinical outcomes.

Supplementary Material

Refer to Web version on PubMed Central for supplementary material.

Acknowledgements

NC was supported by T32CA009685 and a Young Investigator Award from the American Head and Neck Society. RJW was supported by R01CA15786 and R01CA219534. Memorial Sloan-Kettering Cancer Center Core Facilities were supported by P30CA008748. We thank Y. Romin and S. Fujisawa for assistance with microscopy, H. Carl Le and J. Koutcher for assistance with small animal MRI imaging, and I. Linkov for assistance with immunostaining.

References

1. Batsakis JG. Nerves and neurotropic carcinomas. Ann Otol Rhinol Laryngol, 1985 94:426–27. [PubMed: 4026129]
2. Liebig C, et al. Perineural invasion in cancer: a review of the literature. Cancer, 2009; 115:3379–91. [PubMed: 19484787]

3. Bapat AA, Hostetter G, Von Hoff DD, Han H. Perineural invasion and associated pain in pancreatic cancer. Nat Rev Cancer, 2011; 11:695–707. [PubMed: 21941281]
4. Fagan JJ, et al. Perineural invasion in squamous cell carcinoma of the head and neck. Arch Otolaryngol Head Neck Surg, 1998; 124:637–40. [PubMed: 9639472]
5. Beard CJ, et al. Perineural invasion is associated with increased relapse after external beam radiotherapy for men with low-risk prostate cancer and may be a marker for occult, high-grade cancer. Int J Radiat Oncol Biol Phys, 2004; 58:19–24. [PubMed: 14697416]
6. Law WL, Chu KW. Anterior resection for rectal cancer with mesorectal excision: a prospective evaluation of 622 patients. Ann Surg, 2004; 240:260–268. [PubMed: 15273550]
7. Soo KC, Carter RL, O'Brien CJ. Prognostic implications of perineural spread in squamous cell carcinomas of the head and neck. Laryngoscope, 1986; 96:1145–1148. [PubMed: 3762289]
8. Kurtz KA, Hoffman HT, Zimmerman MB. Perineural and vascular invasion in oral cavity squamous carcinoma: increased incidence on re-review of slides and by using immunohistochemical enhancement. Arch Pathol Lab Med. 2005; 129:354–9. [PubMed: 15737030]
9. Goepfert H, Dichtel WJ, Medina JE, Lindberg RD, Luna MD. Perineural invasion in squamous cell skin carcinoma of head and neck. Am J Surg 1984; 148:542–547. [PubMed: 6486325]
10. Leibig C, Ayala G, Wilks J, Verstovsek G, Liu H, Agrawal N, Berger DH, Albo D. Perineural invasion is an independent predictor of outcome in colorectal cancer. 2009;JCO 27:5131–37.
11. Paratcha G, Ledda F. GDNF and GFR-α: a versatile molecular complex for developing neurons. Trends in Neurosciences, 2008; 31:384–391. [PubMed: 18597864]
12. Gil Z, Cavel O, Kelly K, Brader P, Rein A, Gao SP, Carlson DL, Shah JP, Fong Y, Wong RJ. Paracrine regulation of pancreatic cancer cell invasion by peripheral nerves. J Natl Cancer Institute, 2010; 102:107–118.
13. He S, Chen CH, Chernichenko N, He S, Bakst RL, Barajas F, Deborde S, Allen PJ, Vakiani E, Yu Z, Wong RJ. GFRα1 released by nerves enhances cancer cell perineural invasion through GDNF-RET signaling. Proc Natl Acad Sci U S A. 2014; 111:E2008–17. [PubMed: 24778213]
14. Veit C, Genze F, Menke A, Hoeffert S, Gress TM, Gierschik P, Giehl K. Activation of phosphatidylinositol 3-kinase and extracellular signal-related kinase is required for glial-derived neurotrophic factor-induced migration and invasion of pancreatic cells. Cancer Res. 2004; 64:5291–5300. [PubMed: 15289335]
15. Nobes CD, Hall A. Rho GTPases control polarity, protrusion and adhesion during cell movement. J Cell Biol. 1999; 144:1235–1244. [PubMed: 10087266]
16. Jaffe AB, Hall Alan, A. Rho GTPases: biochemistry and biology. Ann Rev Cell Dev Biol. 2005; 21:247–69. [PubMed: 16212495]
17. Parri M, Chiarugi P. Rac and Rho GTPases in cancer cell motility control. Cell Comm and Signal. 2010; 8:23.
18. Fritz G, Brachetti C, Bahlmann F, Schmidt M, Kaina B. Rho GTPases in human breast tumors: expression and mutation analyses and correlation with clinical parameters. Br J Cancer. 2002; 87:635–44. [PubMed: 12237774]
19. Vega FM, Ridley AJ. Rho GTPases in cancer cell biology. FEBS Lett. 2008; 582:2093–101. [PubMed: 18460342]
20. Orgaz JL, Herraiz C, Sanz-Moreno V. Rho GTPases modulate malignant transformation of tumor cells. Small GTPases. 2014; 5:e29019. [PubMed: 25036871]
21. Barrio-Real L, Kazanietz MG. Rho GEFs and cancer: linking gene expression and metastatic dissemination. Sci Signal. 2012; 5:pe43. [PubMed: 23033535]
22. Reymond N, Im JH, Garg R, Vega FM, Borda d'Agua B, Riou P, Cox S, Valderrama F, Muschel RJ, Ridley AJ. Cdc42 promotes transendothelial migration of cancer cells through β1 integrin. J Cell Biol. 2012; 199:653–68. [PubMed: 23148235]
23. He S, He S, Chun CH, Deborde S, Bakst RL, Chernichenko N, McNamara WF, Lee SY, Barajas F, Yu Z, Al-Ahmadie HA, Wong RJ. The chemokine (CCL2-CCR2) signaling axis mediates perineural invasion. Mol Cancer Res. 2015; 13:380–390. [PubMed: 25312961]
24. Ayala GE, Wheeler TM, Shine HD, Schmelz M, Frolov A, Chakraborty S, Rowley D In vitro dorsal root ganglia and human prostate cell line interaction: redefining perineural invasion in prostate cancer. Prostate. 2001; 49:213–223. [PubMed: 11746267]

25. Bakst RL, Lee N, He S, Chernichenko N, Chen CH, Linkov G, Le CH, Koutcher J, Vakiani E, Wong RJ. Radiation impairs perineural invasion by modulating the nerve microenvironment. PLoS One. 2012; 7:e39925. [PubMed: 22768171]
26. Deborde S, Omelchenko T, Lyubchik A, Zhou Y, He S, McNamara WF, Chernichenko N, Lee SY, Barajas F, Chen CH, Bakst RL, Vakiani E, He S, Hall A, Wong RJ. Schwann cells induce cancer dispersion and invasion. J Clin Invest. 2016; 126:1529–1554.
27. Bakst RL, Xiong H, Chen CH, Deborde S, Lyubchik A, Zhou Y, He S, McNamara WF, Lee SY, Olson OC, Leiner IM, Marcadis AR, Keith JW, Al-Ahmadie HA, Katabi N, Gil Z, Vakiani E, Joyce JA, Pamer E, Wong RJ. Inflammatory monocytes promote perineural invasion via CCL2-mediated recruitment and cathepsin B expression. Cancer Res. 2017; 77:6400–6414. [PubMed: 28951461]
28. Merlot S, Firtel RA. Leading the way: directional sensing through phosphatidylinositol 3-kinase and other signaling pathways. J Cell Sci. 2003; 116:3471–8. [PubMed: 12893811]
29. Riento K, Ridley AJ. Rocks: multifunctional kinases in cell behavior. Nat Rev Mol Cell Biol. 2003; 4:446–56. [PubMed: 12778124]
30. Etienne-Manneville S, Hall. Cdc42 regulates GSK-3beta and adenomatous polyposis coli to control cell polarity. Nature. 2003; 421:743–6.
31. Petrie RJ, Doyle AD, Yamada KM. Random versus directionally persistent cell migration. Nat Rev Mol Cell Biol. 2009; 10:538–49. [PubMed: 19603038]
32. Stengel K, Aheng Y. Cdc42 in oncogenic tranformation, invasion, and tumorigenesis. Cell Signal. 2011; 23:1415–23. [PubMed: 21515363]
33. Allen WE, Zicha D, Ridley A, Jones GE. A role for Cdc42 in macrophage chemotaxis. J Cell Biol. 1998; 141:1147–57. [PubMed: 9606207]
34. Roussos ET, Condeelis JS, Patsialou A. Chemotaxis in cancer. Nat Rev Cancer. 2011 11:573–587. [PubMed: 21779009]
35. Gaggioli C, Hooper S, Hidalgo-Carcedo C, Grosse R, Marshall JF, Harrington K, Sahai E. Fibroblast-led collective invasion of carcinoma cells with differing roles for RhoGTPases in leading and following cells. Nat Cell Biol. 2007; 9:1392–400. [PubMed: 18037882]
36. Osmani N, Vitale N, Borg JP, Etienne-Manneville S. Scrib controls Cdc42 localization and activity to promote cell polarization during astrocyte migration Curr Biol. 2006; 16:2395–2405. [PubMed: 17081755]
37. Osmani N, Peglion F, Chavrier P, Etienne-Manneville S. Cdc42 localization and cell polarity depend on membrane traffic. J Cell Biol. 2010; 191:1261–9. [PubMed: 21173111]
38. Rohatji R, Ma L, Miki H, Lopez M, Kirchhausen T, Takenawa T, Kirschner MW. The Interaction between N-WASP and the Arp2/3 complex links Cdc42-dependent signals to actin assembly. Cell. 1999; 97:221–31. [PubMed: 10219243]
39. Guo JC, Li J, Zhao YP, Zhou L, Cui QC, Zhou WX, Zhang TP, You L, Shu H. N-WASP in pancreatic ductal adenocarcinoma: associations with perineural invasion and poor prognosis. World J Surg. 2014; 38:2126–31. [PubMed: 24718883]

Implications:

Cdc42 regulates cancer cell directional migration towards and along nerves in perineural invasion.

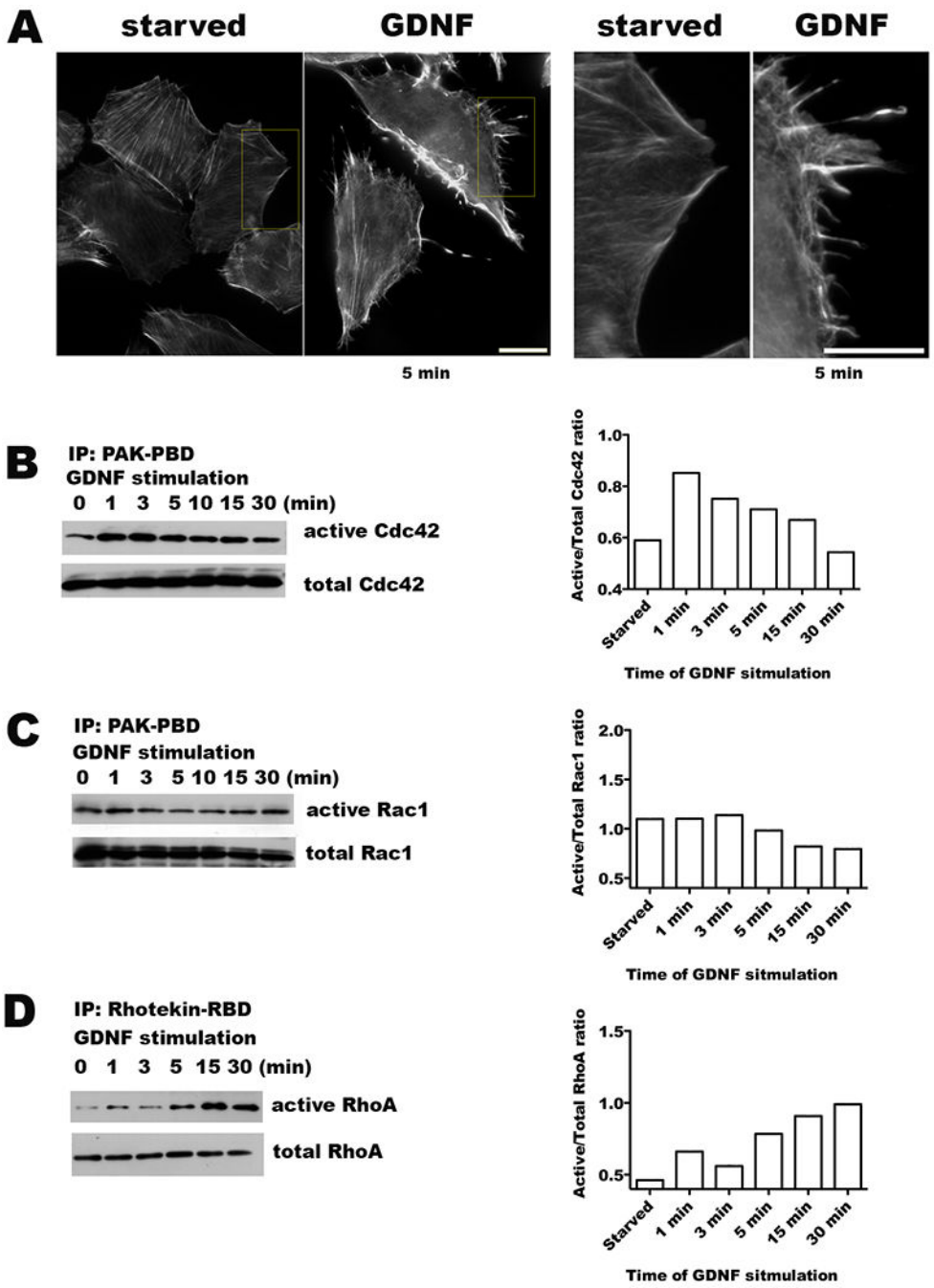

Figure 1. Activation of Rho GTPases by glial cell line-derived neurotrophic factor (GDNF).

A. Serum starved MiaPaCa2 cells were exposed to 100 ng/ml of GDNF for 5 minutes and then fixed in formaldehyde. Actin filaments were visualized with rhodamine-phalloidin staining, demonstrating the development of microspikes, filipodia, and stress fibers. Serum starved cells not exposed to GDNF were used as a control. (Scale bar = 15 μm) B-D. Western blots of GST pull-down assays assess for changes in the active, GTP-bound forms of Cdc42, Rac1, and RhoA in response to exposure to GDNF (100 ng/ml) with corresponding quantification by densitometry.

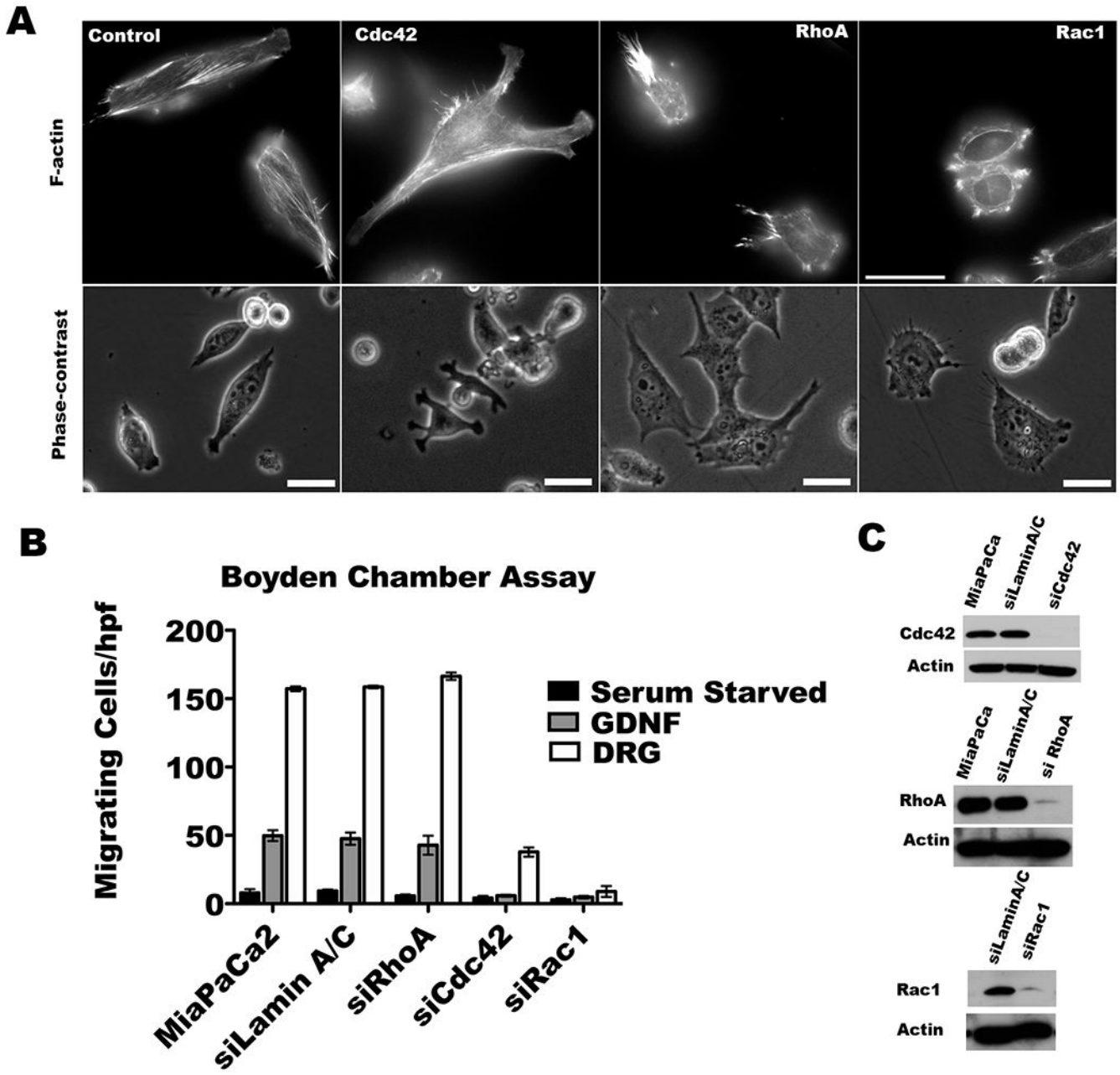

Figure 2. Cdc42 and Rac1 silencing alters MiaPaCa2 cytoskeletal structure and impairs GDNF dependent chemotaxis.

A. MiaPaCa2 cells were transfected with the indicated siRNA SMARTpools. Actin filaments were visualized with rhodamine-phalloidin staining. Cdc42 depletion results in lamellipodial protrusion formation in multiple different directions simultaneously. Rac1 inhibition impairs lamellipodial protrusion formation. RhoA depleted cells tend to retain unidirectional lamellipodial protrusions. (Scale bar = 30 μm). B. Serum-starved siRNA transfected Cdc42, Rac1, RhoA, or LaminA/C (control) MiaPaCa2 cells underwent Boyden chamber assays using GDNF (100 ng/ml) or dorsal root ganglia (DRG) in the lower chamber as an attractant over 24 hours. DRG were stronger than GDNF as an attractant. Cdc42 or

Rac1 silencing impairs chemotaxis towards DRG as compared with either MiaPaCa2 or siLamin A/C as control ($p<0.05$ for all comparisons, t-test), while RhoA depletion has no effect (p=NS). C. Western blots of Cdc42, Rac1, and RhoA confirm protein depletion in the siRNA SMARTpool transfected cells.

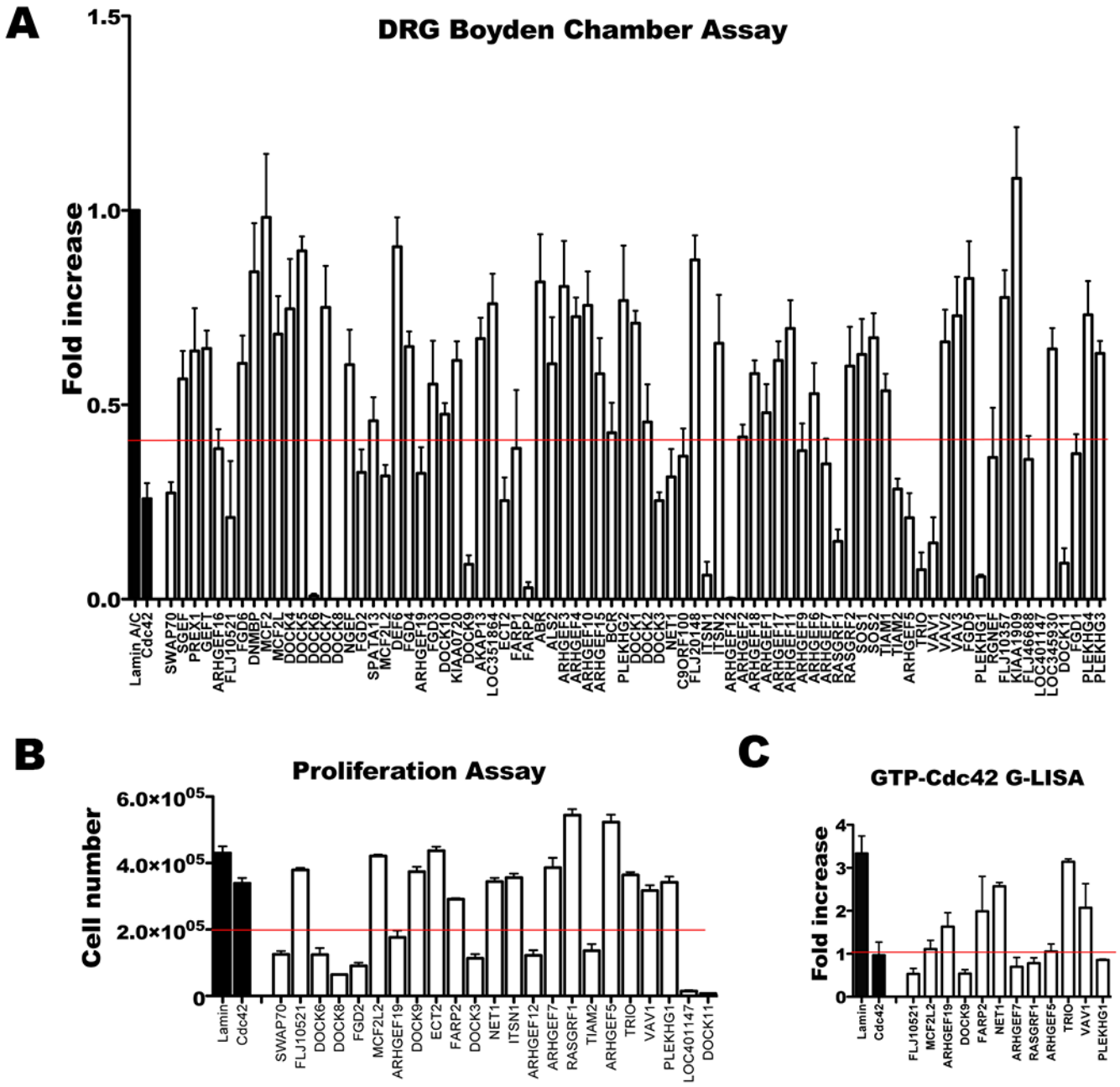

Figure 3. Identification of Rho GTPase GEFs necessary for migration and Cdc42 activation using an siRNA based screen.

A. MiaPaCa2 cells were transiently transfected with individual siRNA from a GEF siRNA library, and migration towards DRG by Boyden chamber assay was measured. The GEFs required for migration (below the red line) were selected. B. Cell proliferation was assessed following siRNA transfection of selected GEFs to exclude the GEFs required for proliferation. Resulting GEF candidates (above the red line) were selected. ECT2 was excluded because silencing resulted in a multinucleated cell phenotype. C. Each GEF candidate underwent siRNA tranfection followed by quantification of GTP-Cdc42 (active Cdc42) by G-LISA following stimulation with GDNF. The final 6 GEFs (below the red line)

meet the criteria of: (1) driving cancer cell migration towards DRG, (2) not required for cell proliferation, and (3) activating Cdc42.

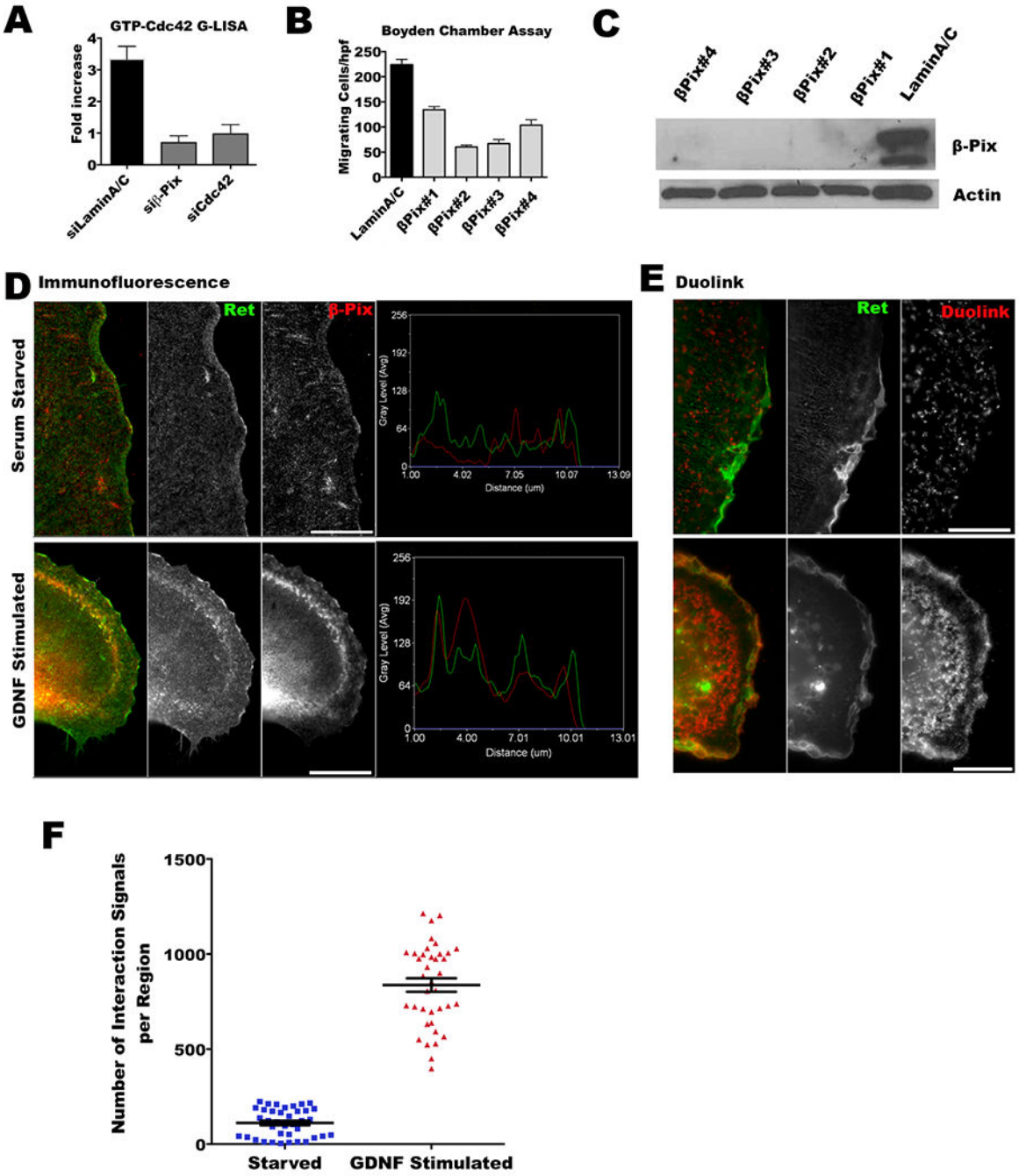

Figure 4. β-Pix interacts directly with RET upon GDNF stimulation.

A. Depletion of β-Pix in MiaPaCa-2 cells results in decreased active GTP-Cdc42 under GDNF stimulation. Significant differences in active GTP-Cdc42 between siLamin A/C and siCdc42 ($p<0.05$, t-test), and between siLamin A/C and si-β-pix ($p<0.05$, t-test) were identified. B. Depletion of β-Pix in MiaPaCa2 cells using four different siRNA duplexes impairs MiaPaCa2 cell migration towards DRG in Boyden chamber assays as compared with siLamin A/C ($p<0.05$, all comparisons, t-test). C. Western blots were performed to validate β-Pix depletion in siRNA transfected MiaPaCa2. D. β-Pix co-localizes with RET

under GDNF stimulation in Caco2 cells transfected with GFP-RET and HA-β-Pix. Immunofluorescence for HA-β-Pix (red) and GFP-RET (green) with and without GDNF stimulation was assessed. The line scan function of Metamorph shows strong co-localization of the two signals under GNDF stimulation, but not at baseline conditions. E. Proximity ligation assay was performed to confirm direct interaction and co-localization between β-Pix and RET in Caco2 cells under GDNF stimulation. Images were obtained by epifluorescence microscopy. F. Puncta indicating β-Pix and RET interactions by proximity ligation assay were counted using MetaMorph software, with threshold signal sizes ranging from 0.5–2.5 μm. A significantly higher number of β-Pix and RET interactions were detected under GDNF stimulation ($p<0.05$, t-test).

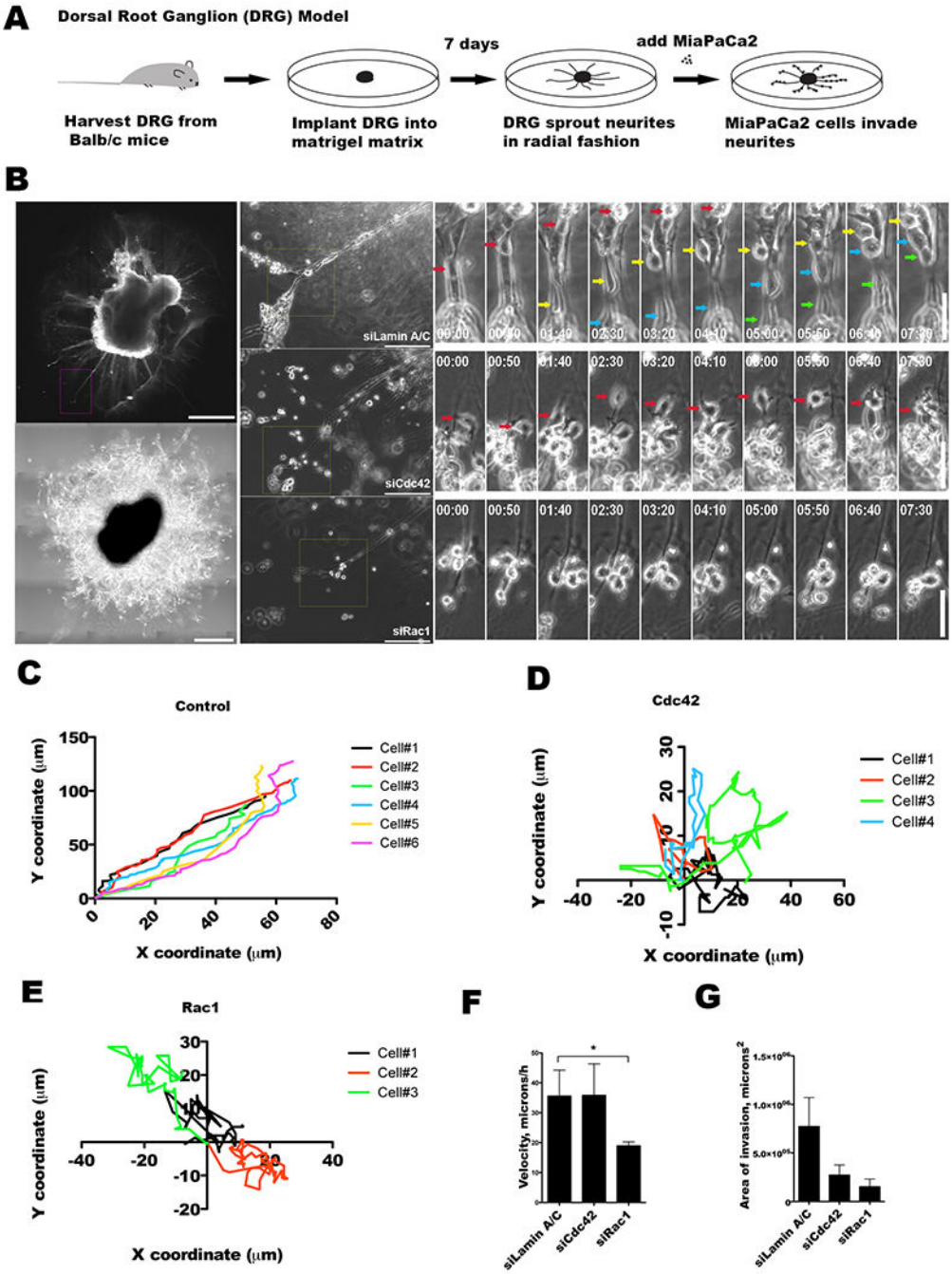

Figure 5. Cdc42 regulates the direction of cancer cell migration along nerves.

A. Dorsal root ganglia (DRG) were harvested from mice, grown in Matrigel, and co-cultured with MiaPaCa2 cancer cells as an *in vitro* model to explore cancer and nerve interactions. B. DRG implanted in Matrigel develops axonal projections or neurites, as imaged by immunofluorescence confocal microscopy using Tuj1 antibody (scale bar = 200 μm, left upper panel), or phase contrast microscopy, (scale bar = 400 μm, left lower panel). Representative MiaPaCa2 cells treated with siLaminA/C (upper central panel), siCdc42 (mid central panel), or siRac1 (lower central panel) are examined when associated with DRG

neurites (scale bar = 200 μm). High power, sequential, time-lapse micrographs are shown (scale bar = 100 μm, right panels). Control siLaminA/C (right upper panels), siCdc42 (right mid panels), and siRac1 (right lower panels) MiaPaCa2 cells are depicted with colored arrows marking the migrating cells. C-E. Coordinate graphs depicting the single cell migration trajectories of control siLaminA/C (C), siCdc42 (D), and siRac1 (E) MiaPaCa2 cells. The siLaminA/C cells demonstrate consistent migration along the direction of the DRG neurites. The siCdc42 and siRac1 cells both exhibit a loss of directional migration. F. The average speed of single cell migration was calculated for the siLaminA/C, siCdc42, and siRac1 groups. Speed was maintained in the siLaminA/C and siCdc42 cells, but was significantly diminished in the siRac1 cells. G. The average area of DRG invasion was measured for siLaminA/C, siCdc42 and siRac1 cells after 48 hours of co-culture. Silencing of Cdc42 ($p=0.08$) or Rac1 ($p=0.07$) as compared with siLamin A/C resulted in a trend towards a decrease in the area of PNI.

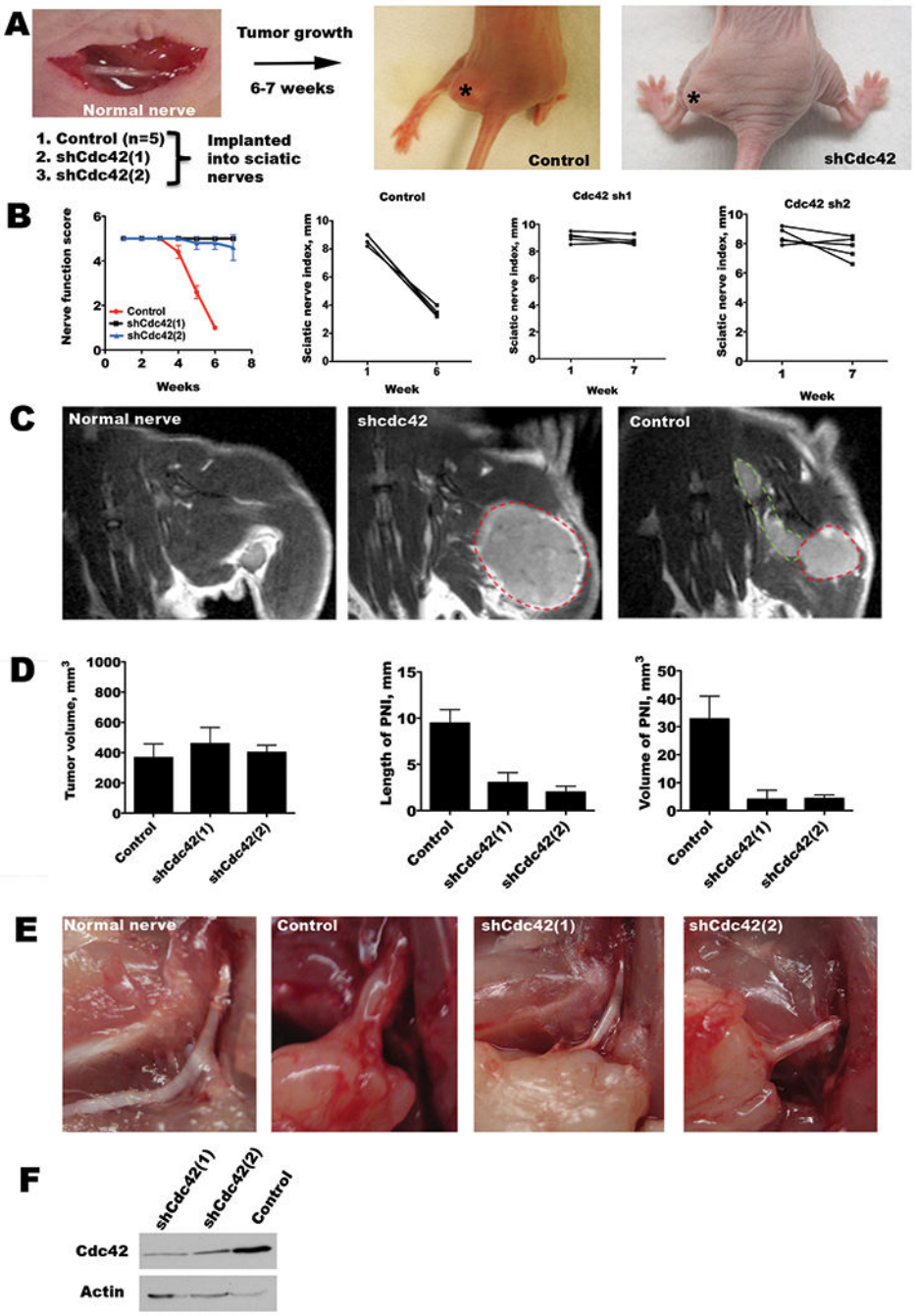

Figure 6. Cdc42 regulates perineural invasion in vivo.

A. An *in vivo* model of PNI involves the implantation of cancer cells into murine sciatic nerves. Stable MiaPaCa2 cell lines were generated with shRNA targeting Cdc42 or empty vector transfected controls. Representative images of mice 6 weeks after tumor implantation show left hind limb paralysis in the control tumor group, but normal limb function in the shCdc42 groups. Asterisks indicate the location of the sciatic nerve tumor. B. Sciatic nerve function was assessed by both the sciatic nerve function score (hind limb function), and the sciatic nerve index (hind paw width). Mean scores for sciatic nerve function score show a

significant decline over 6 weeks for the control group ($p<0.05$, t-test), but not for the shCdc42 groups (p=NS, t-test). Similarly, the control group showed a significant decline in sciatic nerve index ($p<0.05$, t-test), but not for the shCdc42 groups (p=NS, t-test). To account for differential growth rates, comparisons were made between equivalent tumor volumes between week 6 data for the control group, and week 7 in the shCdc42 groups. C. Magnetic resonance images (MRI, T1 with gadolinium) are shown of a representative, non-injected, sciatic nerve (no tumor), an shCdc42 sciatic nerve tumor (lacking PNI), and a control sciatic nerve tumor (with PNI). The primary tumor is outlined in red, and the perineural component is outlined in green. D. Quantification of the primary tumor volume, the length of PNI, and the volume of tumor in the region of PNI by MRI. Comparisons were performed between week 6 for the control group, and week 7 in the shCdc42 groups when mean volumes were similar (p=NS, t-test). This comparison at different time points accounts for differences in tumor growth rate. Both the length of PNI and volume of tumor in the PNI were significantly reduced in both shCdc42 groups as compared with control ($p<0.05$ for both comparisons, for both shCdc42(1) and shCdc42(2), t-test). E. *In-situ* image of a surgically exposed sciatic nerve in a non-injected mouse, with control at week 6, and shCdc42(1) and shCdc42(2) tumors at week 7. Only the control has significant sciatic nerve thickening, consistent with perineural invasion, although all tumor groups developed equivalent primary tumor volume. F. Western blot of shCdc42(1) and shCdc42(2) MiaPaCa2 cell lines shows Cdc42 depletion as compared with control.

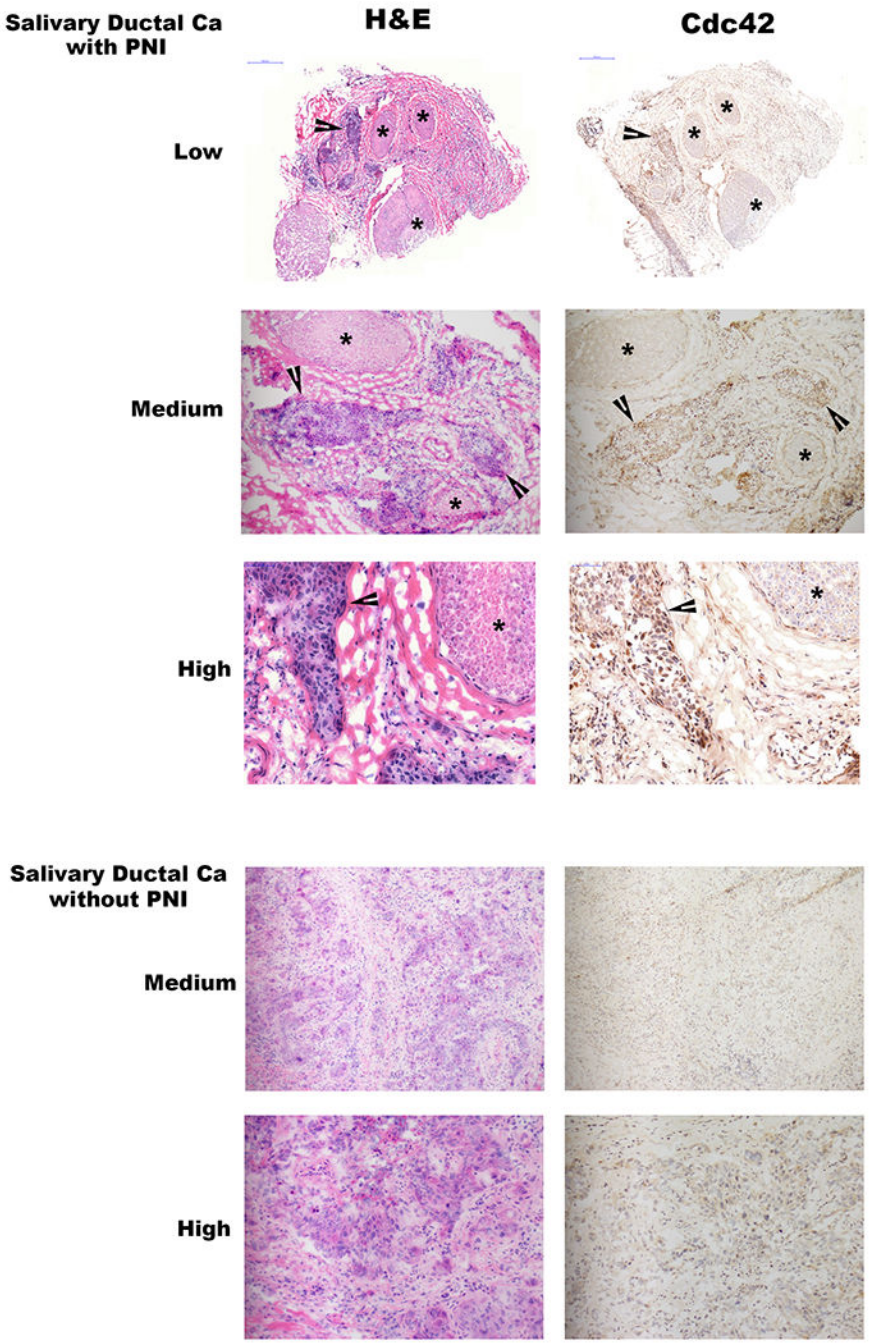

Figure 7. GTP-Cdc42 expression in human neuroinvasive carcinomas.

Low (20x), medium (100x), and high (200x) power magnification hematoxylin and eosin (H&E) and GTP-Cdc42 immunohistochemistry (IHC) staining of two different human salivary ductal carcinoma specimens, one with and one without perineural invasion. Asterisks indicate nerve fascicles, while arrowheads indicate sites of carcinoma. Photomicrographs demonstrate active Cdc42 in cancer cells that are invading nerves, but diminished Cdc42 expression in cancer cells lacking perineural invasion.